A double peak of the coercive force near the compensation temperature in the rare earth iron garnets

A double peak of the coercive force near the compensation temperature in the rare earth iron garnets

A double peak of the coercive force near the compensation temperature in the rare earth iron garnets

M. UEMURA, T. YAMAGISHI, S. EBISU, S. CHIKAZAWA

and S. NAGATA*

Department of Materials Science and Engineering, Muroran Institute of Technology, 27-1 Mizumoto-cho, Muroran, Hokkaido, 050-8585, Japan

Abstract

The behavior of the coercive force, H_c, of ferrimagnets near the compensation temperature, T_{comp}, for polycrystalline rare earth iron garnets $R_3Fe_5O_{12}$ (R = Gd, Tb, Dy, Ho and Er) has been studied in detail. The present experimental results have verified the double peak in H_c near T_{comp} for these rare earth iron garnets $R_3Fe_5O_{12}$. For $Dy_3Fe_5O_{12}$, the experimental values are T_{comp} = 224 K, H_c (max) = 600 Oe at $T_{comp} \pm$ K and $\approx$ 10 K. The two peaks of H_c arise at 214 and 232 K. The appearance of the double peak of H_c is an intrinsic and characteristic property for $R_3Fe_5O_{12}$. The results can be understood on the basis of a simple model. The hysteresis loop in the magnetization is caused by rotation of single domain under the influence of crystalline anisotropy rather than domain wall displacements of the multi-domain structure. The rare earth ion behaves as superimposed paraprocess under the influence of weak exchange field produced by iron sublattices and an external magnetic field.

*Corresponding author. E-mail: naga-sho@mmm.muroran-it.ac.jp

1. Introduction

The garnet structure was originally solved by Menzer [1]. A number of garnet structure refinements have been made. Garnet-type compounds have attracted much interest in their magnetic properties both the theoretically and via experiments, in particular, ferrimagnetism of the rare earth iron garnets [2-10]. A detailed review is provided by Hellwege [11]. There have been some recent important reports, e.g. the discovery of anomalous peaks in $Ho_3Al_5O_{12}$ due to a phase transition [12], the Van Vleck temperature-independent paramagnetic susceptibility of $Tm_3Al_5O_{12}$ [13], the abnormal susceptibility of vanadium garnets $NaPb_2Co_2V_3O_{12}$ [14] and $AgCa_2Co_2V_3O_{12}$ [15, 16].

Figure 1 shows the garnet structure has cubic symmetry with space group $Ia\bar{3}d$ (No. 232, O_h^{10}) [1, 10, 15]. The general chemical formula of garnet compounds can be written as $\{C\}_3[A]_2(D)_3O_{12}$, where C, A and D sites are cation sites. These three cation sites are surrounded by oxygen ions (O^{2-}) at dodecahedron, octahedron and tetrahedron positions, respectively. The rare earth iron garnets can be written as $R_3Fe_5O_{12}$, where C sites are occupied by trivalent rare earth ion R^{3+} and A and D sites by Fe^{3+}.

The rare earth iron garnet exhibit ferrimagnetisms and has so-called compensation temperature, T_{comp}, at which the sublattice magnetizations cancel each other and the resultant magnetization becomes zero. The magnetic moment of R^{3+} ions is opposite to the resultant of the Fe^{3+} ions and overrides that of resultant of Fe^{3+} ion at low temperatures. With increasing temperature, the magnetization of R^{3+} ions falls off more quickly than that of the A-and D-sublattices because of the coupling due to weak exchange field produced by iron sublattices. There is no net moment at T_{comp}. Above T_{comp} the magnetization of Fe^{3+} ion sublattices predominates. The magnetization of the resultant iron sublattices does not depend on the external field because of high Curie temperature of 559 K, whereas the magnetization of the R^{3+} ion sublattice is markedly affected by the external field with superimposed Curie-Weiss law (so-called paraprocess magnetization).

In previous work we investigated the ferromagnetic order in the mixed garnet $(Y_{1-x}Gd_x)_3Fe_5O_{12}$ system [17]. An enlargement of coercive force H_c in the hysteresis loop for the low-field M-H curve is clearly observed in near T_{comp} [17]. The coercive force H_c is defined as that value of magnetizing field that causes the magnetization of the specimen to be zero. Many earlier researchers have also investigated the temperature dependence of the cohesive force near T_{comp} for $Gd_3Fe_5O_{12}$. The problem remains a controversy subject. Whereas one study on $Gd_3Fe_5O_{12}$ showed that it exhibits a single peak in H_c as a function of temperature [18], the others revealed a double peak in H_c near T_{comp} [19-25]. The key point is that previous researchers have not presented explicit magnetic behavior (M-H) curves near T_{comp}, which we will do in this paper. One notable exception is the detailed investigation of $Gd_3Fe_5O_{12}$ by Mee [26], who reported that the temperature dependence of the hysteresis loop for single crystals shows a double peak in H_c near T_{comp}. The most significant experimental results of the hysteresis curves are not available for R= Tb, Dy, Ho and Er near T_{comp} so far. Hence, the hysteresis curves and the temperature dependence of H_c were measured directly for the several rare earth iron garnets.
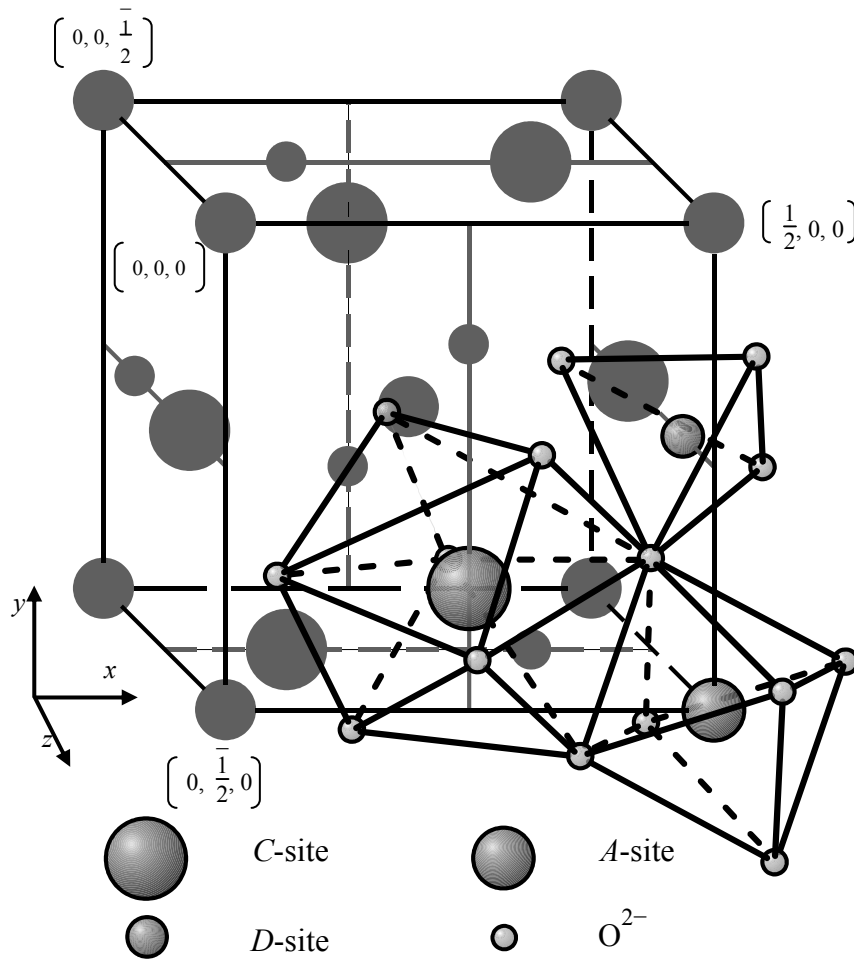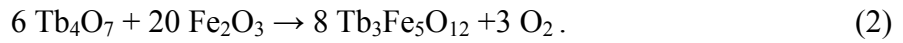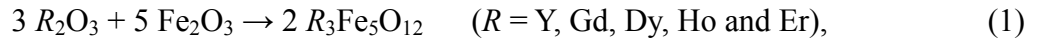
Figure 1. Garnet-type structure has cubic symmetry of space group *Ia*3*d* (No. 232, O_h^{10}) with general chemical formula $\{C\}_3[A]_2(D)_3O_{12}$.

This paper will present systematic results of hysteresis *M-H* curves near T_{comp} for polycrystalline rare earth iron garnets (R= Gd, Tb, Dy, Ho and Er). These hysteresis curves near T_{comp} are reported here for the first time except the R= Gd [26]. As a representative observation, the detailed results for $Dy_3Fe_5O_{12}$ are displayed, demonstrating a double peak of H_c near T_{comp}. Our measurements verify that the maximum of H_c splits into two peaks. It is stressed that the effect of the double peak in H_c near T_{comp} for $R_3Fe_5O_{12}$ is an intrinsic general feature of the rare earth iron garnets. These results have been understood on the basis of a simple model of single domain structure where the magnetization reversal is caused by single domain rotation under the influence of the crystalline anisotropy rather than domain wall displacements of the multi-domain structure. Furthermore it should be noted that the rare earth ion behaves as paramagnetically under the influence of an external magnetic field, and weak exchange field produced by iron sublattices. This large variation of the magnitude of the paraprocess magnetization of the rare earth ion has a strong effect in the hysteresis curve. The measurements for $Tm_3Fe_5O_{12}$ and $Yb_3Fe_5O_{12}$ are not carried

out in this study because a clear T_{comp} has not observed [9]. The present work has been systematically made for the polycrystalline rare earth iron garnets.

2. Experimental methods

The powder specimens of $R_3Fe_5O_{12}$ (R = Y, Gd, Tb, Dy, Ho and Er) were prepared through solid-state chemical reactions:

$$3 R_2O_3 + 5 Fe_2O_3 \rightarrow 2 R_3Fe_5O_{12} \quad (R = Y, Gd, Dy, Ho \text{ and } Er), \quad (1)$$

$$6 Tb_4O_7 + 20 Fe_2O_3 \rightarrow 8 Tb_3Fe_5O_{12} + 3 O_2. \quad (2)$$

The starting materials, Y_2O_3 (purity 99.99 %), Gd_2O_3 (99.99 %), Tb_4O_7 (99.9 %), Dy_2O_3 (99.9 %), Ho_2O_3 (99.9 %), Er_2O_3 (99.99 %) and Fe_2O_3 (99.9 %), were mixed in the calculated ratio. Mixed powder materials were put on an alumina boat and heated in a furnace. The temperature was raised to 1723 K and was held in air for 4 h for $Y_3Fe_5O_{12}$ and $Gd_3Fe_5O_{12}$, for 6 h for $Tb_3Fe_5O_{12}$, $Dy_3Fe_5O_{12}$, $Ho_3Fe_5O_{12}$ and $Er_3Fe_5O_{12}$. The resultant specimens were reground, and the process was repeated until homogeneous pure phase was obtained.

X-ray powder diffraction (XRD) data were taken at room temperature with Cu Kα radiation. The dc magnetization of powder specimens was measured with a superconducting quantum interference device (rf-SQUID) magnetometer over the range of $5.0 \leq T \leq 700$ K for $Y_3Fe_5O_{12}$ and $Gd_3Fe_5O_{12}$, $5.0 \leq T \leq 350$ K for $Tb_3Fe_5O_{12}$, $Dy_3Fe_5O_{12}$, $Ho_3Fe_5O_{12}$ and $Er_3Fe_5O_{12}$.

3. Results and discussion

3.1. *X-ray powder diffraction*

The powder specimens were successfully synthesized for $R_3Fe_5O_{12}$ (R = Y, Gd, Tb, Dy, Ho and Er). The colour of all powder specimens is dark green. Since the diffraction pattern for $Tb_3Fe_5O_{12}$ is lacking and not available on the JCPDS cards, the X–ray powder diffraction pattern for $Tb_3Fe_5O_{12}$ at room temperature is shown in figure 2 as a representative result. The Miller indices, a comparison of d spacings between calculated and the observed values, and the observed peak intensities I_{obs} are listed in table 1. The lattice constant was evaluated to be 12.435 Å for $Tb_3Fe_5O_{12}$ by the least-square method. The lattice constant for $R_3Fe_5O_{12}$ (R = Y, Gd, Tb, Dy, Ho and Er) are listed in table 2.
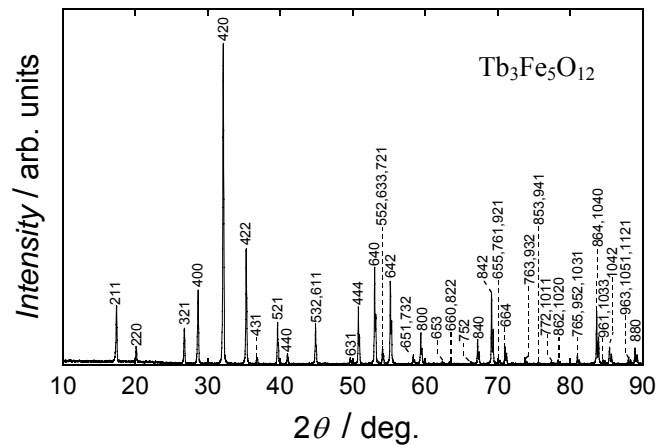
Figure 2. X – ray powder diffraction pattern of $Tb_3Fe_5O_{12}$ at room temperature.
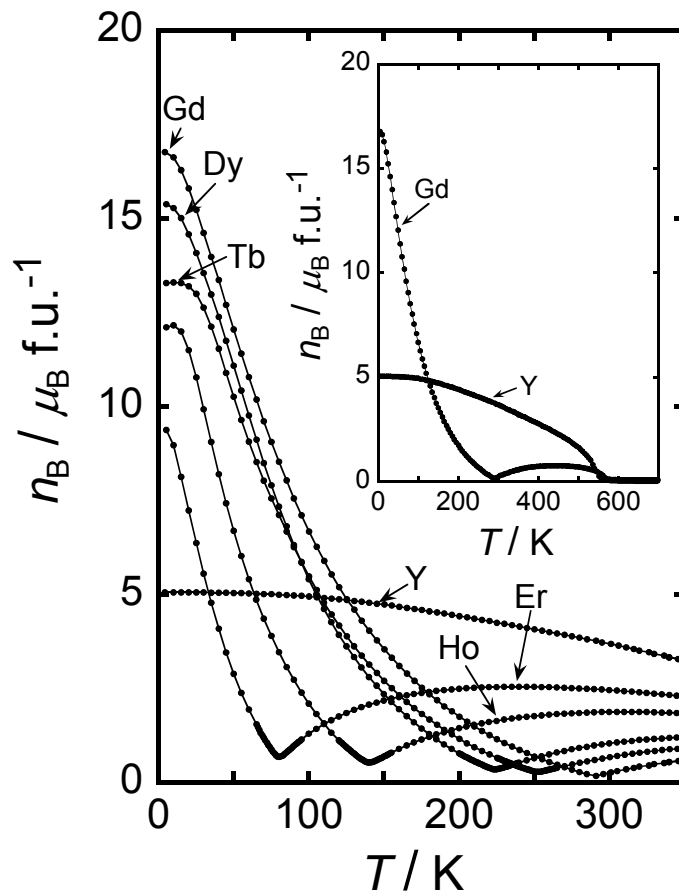

Figure 3. Magnetization in Bohr magnetons per unit formula versus temperature for rare earth iron garnets $R_3Fe_5O_{12}$, R = Y, Gd, Tb, Dy, Ho and Er in a constant field of 10.0 kOe. The inset shows the results of Y and Gd over the temperature range of 5.0 to 700 K.

Table 1. Indices, observed and calculated values of d spacings and observed peak intensities for $Tb_3Fe_5O_{12}$ with the lattice constant $a = 12.435$ Å.

h	k	l	d_{obs} (Å)	d_{cal} (Å)	I_{obs}
2	1	1	5.0866	5.0767	16
2	2	0	4.4054	4.3965	4
3	2	1	3.3262	3.3235	10
4	0	0	3.1122	3.1088	22
4	2	0	2.7827	2.7806	100
4	2	2	2.5405	2.5383	38
5	2	1	2.2718	2.2704	14
4	4	0	2.1995	2.1983	4
5	3	2	2.0179	2.0173	13
6	1	1		2.0173	
6	3	1	1.8343	1.8335	2
4	4	4	1.7958	1.7949	21
6	4	0	1.7251	1.7245	34
5	5	2	1.6926	1.6922	6
6	3	3		1.6922	
7	2	1		1.6922	
6	4	2	1.6626	1.6617	30
6	5	1	1.5799	1.5793	3
7	3	2		1.5793	
8	0	0	1.5552	1.5544	11
6	5	3	1.4870	1.4863	1
6	6	0	1.4663	1.4655	1
8	2	2		1.4655	
7	5	2	1.4086	1.4080	1
8	4	0	1.3908	1.3903	9
8	4	2	1.3572	1.3568	25
6	5	5	1.3413	1.3409	2
7	6	1		1.3409	
9	2	1		1.3409	
6	6	4	1.3258	1.3256	6
7	6	3	1.2829	1.2826	2
9	3	2		1.2826	
8	5	3	1.2565	1.2561	1
9	4	1		1.2561	
7	7	2	1.2317	1.2313	1
10	1	1		1.2313	
8	6	2	1.2195	1.2194	1
10	2	0		1.2194	
7	6	5	1.1858	1.1857	3
9	5	2		1.1857	
10	3	1		1.1857	
8	6	4	1.1548	1.1546	19
10	4	0		1.1546	
9	6	1	1.1450	1.1448	1
10	3	3		1.1448	
10	4	2	1.1354	1.1352	6
9	6	3	1.1081	1.1078	3
10	5	1		1.1078	
11	2	1		1.1078	
8	8	0	1.0994	1.0991	6

Table 2. Lattice constant at room temperature and the compensation temperature T_{comp} for rare earth iron garnets $R_3Fe_5O_{12}$ (R = Y, Gd, Tb, Dy, Ho and Er) in a constant magnetic field of 10.0 kOe.

$R_3Fe_5O_{12}$	lattice constant (Å)	compensation temperature, $T_{comp.}$ (K)
$Y_3Fe_5O_{12}$	12.374	
$Gd_3Fe_5O_{12}$	12.471	290
$Tb_3Fe_5O_{12}$	12.435	252
$Dy_3Fe_5O_{12}$	12.404	224
$Ho_3Fe_5O_{12}$	12.375	140
$Er_3Fe_5O_{12}$	12.349	80

3.2. *Temperature dependence of magnetization at 10. 0 kOe*

Figure 3 shows temperature dependence of the magnetization in Bohr magnetons for $R_3Fe_5O_{12}$ (R = Y, Gd, Tb, Dy, Ho and Er) at an applied magnetic field of 10.0 kOe, over a temperature range from 5.0 to 350 K. The inset shows the results of $Y_3Fe_5O_{12}$ and $Gd_3Fe_5O_{12}$ between 5 and 700 K. Magnetization does not pass through zero at T_{comp} because figure 3 does not indicate the spontaneous magnetization.

Figure 4 displays magnetization curves (*M-H* curves) for $R_3Fe_5O_{12}$ at 5.0 K up to a field of 10.0 kOe in order to make sure the value of the magnetization at 5.0 K. These curves indicate the asymptotic behaviour of approach to saturation in the hysteresis loop. Under a fairly strong magnetic field, $R_3Fe_5O_{12}$ will be magnetized to their saturated state, where all the domain wall displacements in the multi-domain structure have almost finished. It is noted that $Tb_3Fe_5O_{12}$ resists the saturation at rather low field of 10.0 kOe and has a higher value of H_c in comparison with the other garnets. The specimen itself is single phase with high purity, as can be seen in figure 2, therefore, the field is not sufficient to achieve the saturation. In addition, approximately 80 kOe may be sufficient to saturate for the heavier $R_3Fe_5O_{12}$ at 5 K [9].

3.3. *Hysteresis (M-H) curves at several temperatures*

Figures 5 to 9 show magnetization curves for $R_3Fe_5O_{12}$ at T_{comp}, near T_{comp} and 300 K or 400 K in order to evaluate the value of H_c. The value of T_{comp} for $R_3Fe_5O_{12}$ is listed in Table 2. The common characteristics of these hysteresis curves are the real existence of the T_{comp}, at which the sublattice spontaneous magnetizations cancel each other. At T_{comp}, the

variation of the magnetization with applied field can be represented by the linear expression on passing through zero as can be seen in figures 5 to 9, except for $Tb_3Fe_5O_{12}$ as seen in figure 6. We need to find more accurate T_{comp} for $Tb_3Fe_5O_{12}$.

As an example, the figure 5 shows magnetization curves for $Gd_3Fe_5O_{12}$ and enlargement of hysteresis loop is observed at $T_{comp} \pm 10$ K. A hysteresis loop at 400 K is also given as a reference loop far from T_{comp}, where the magnitude of the magnetization is much larger than that near T_{comp} with multi-domain structure.
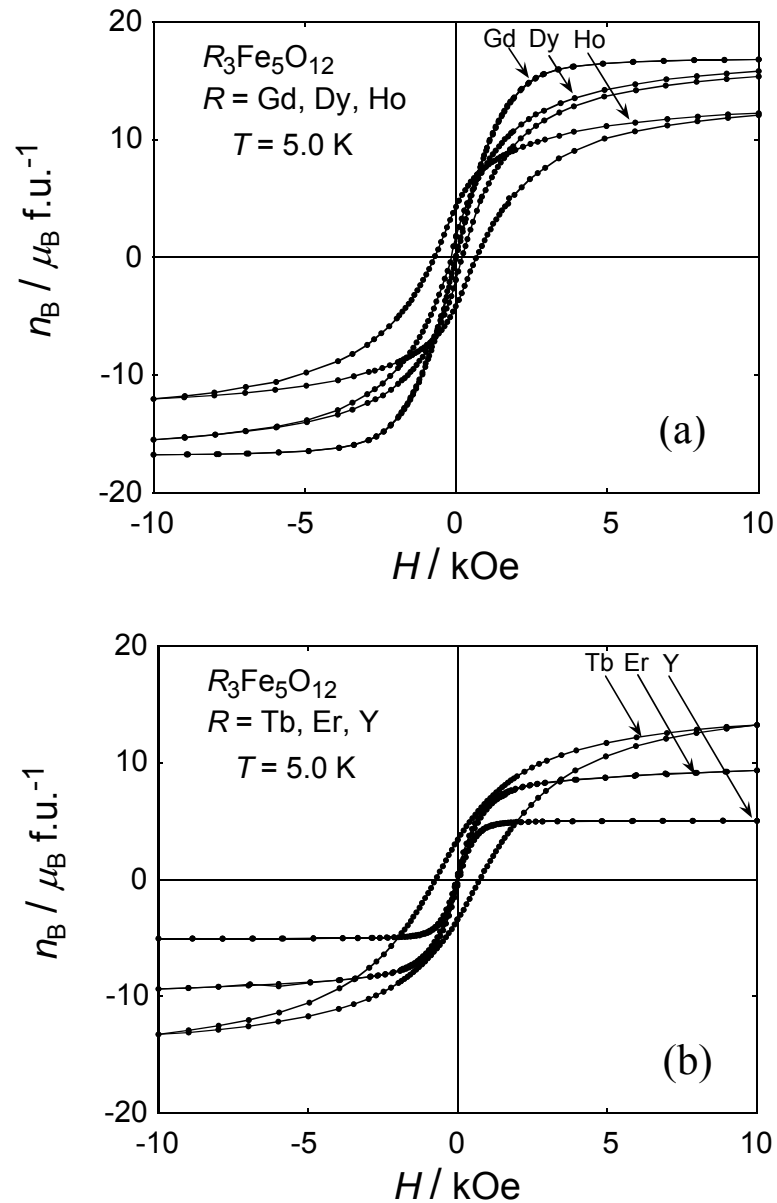

Figure 4.   Magnetic hysteresis curves (M–H curves) for $R_3Fe_5O_{12}$ over the range of applied magnetic field of ± 10.0 kOe, at 5.0 K: (a) R = Gd, Dy and Ho, (b) R = Y, Tb and Er.
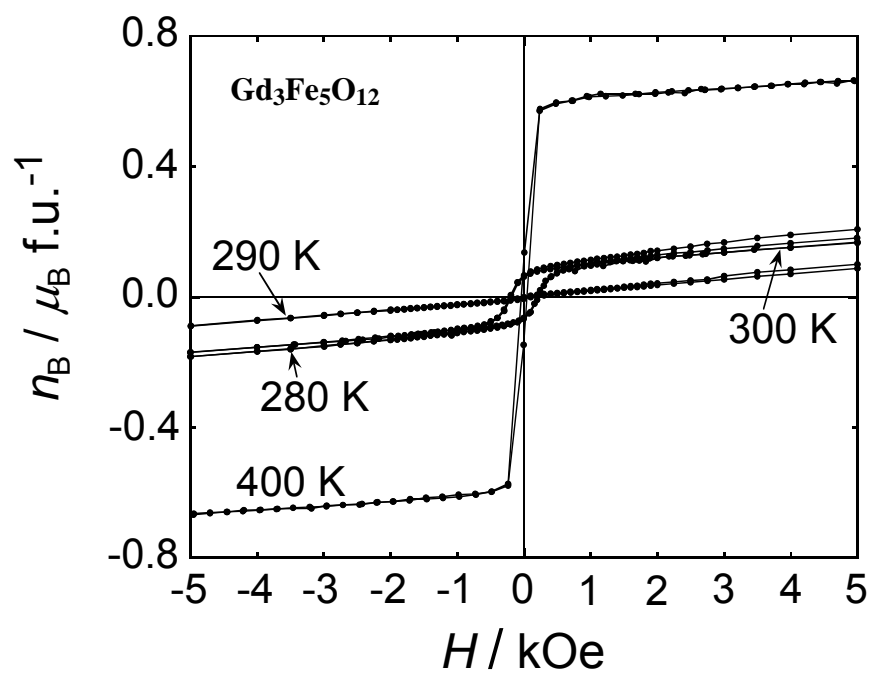
Figure 5. Magnetic hysteresis curves for $Gd_3Fe_5O_{12}$ over the range of applied magnetic field of ± 5.0 kOe, at the several temperatures. The compensation temperature, T_{comp}, is 290 K.

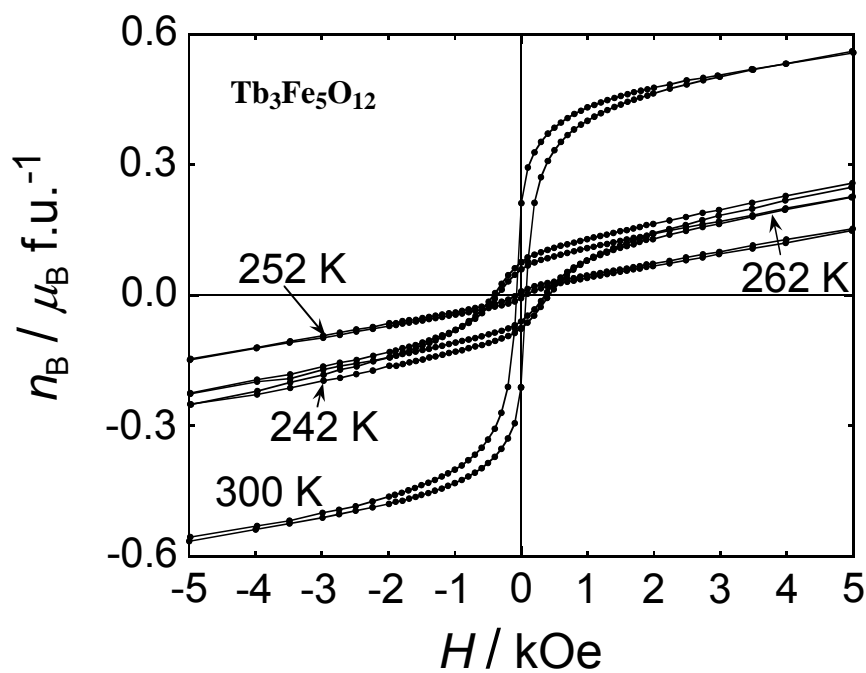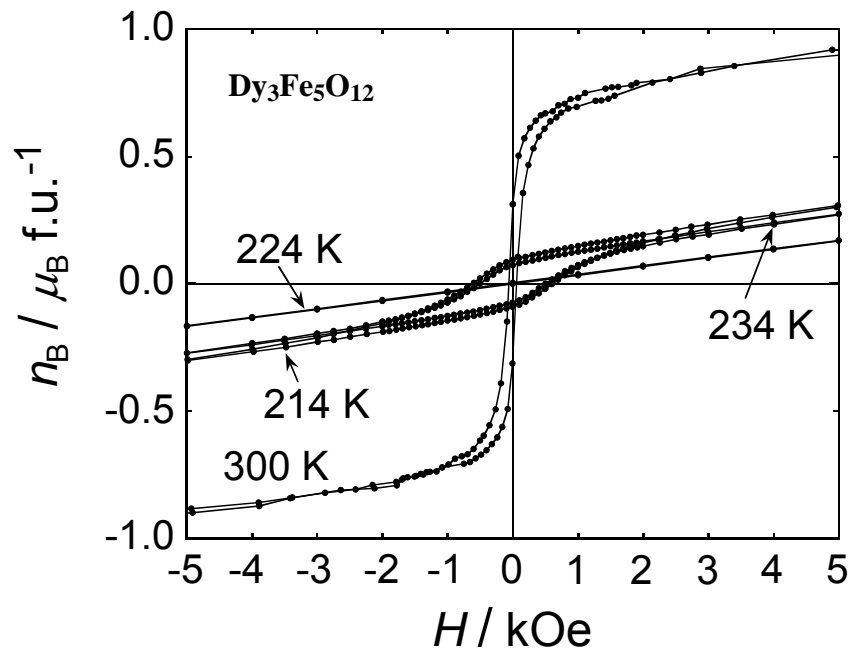Figure 6. Magnetic hysteresis curves for $Tb_3Fe_5O_{12}$ ($T_{comp} = 252$ K).
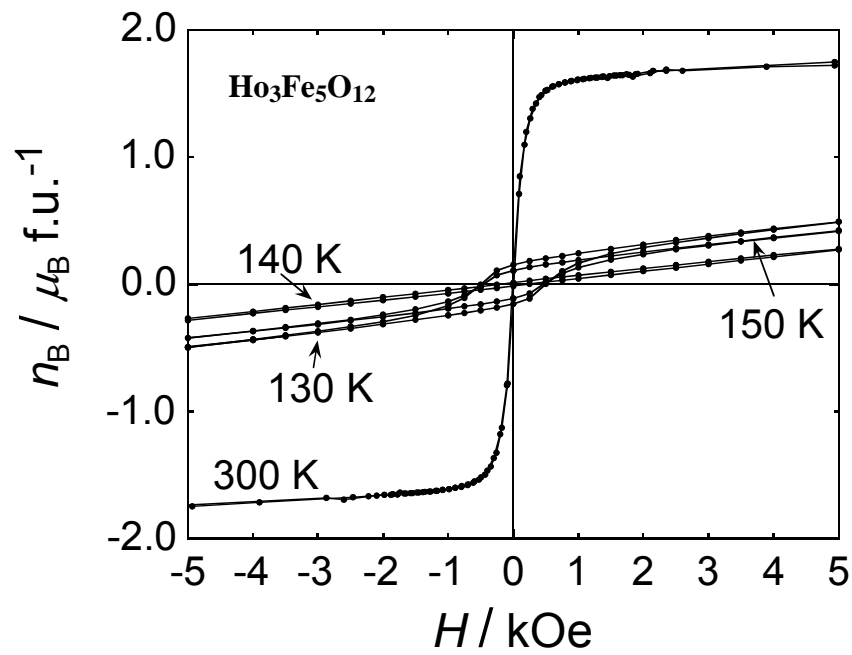
Figure 7.   Magnetic hysteresis curves for $Dy_3Fe_5O_{12}$ (T_{comp} = 224 K).

Figure 8.   Magnetic hysteresis curves for $Ho_3Fe_5O_{12}$ (T_{comp} = 140 K).
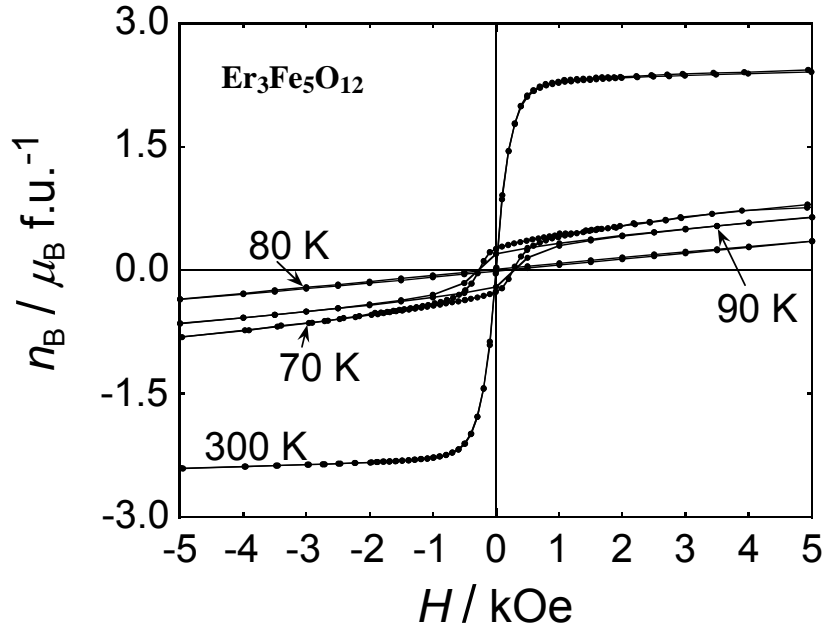
Figure 9.   Magnetic hysteresis curves for $Er_3Fe_5O_{12}$ (T_{comp} = 80 K).

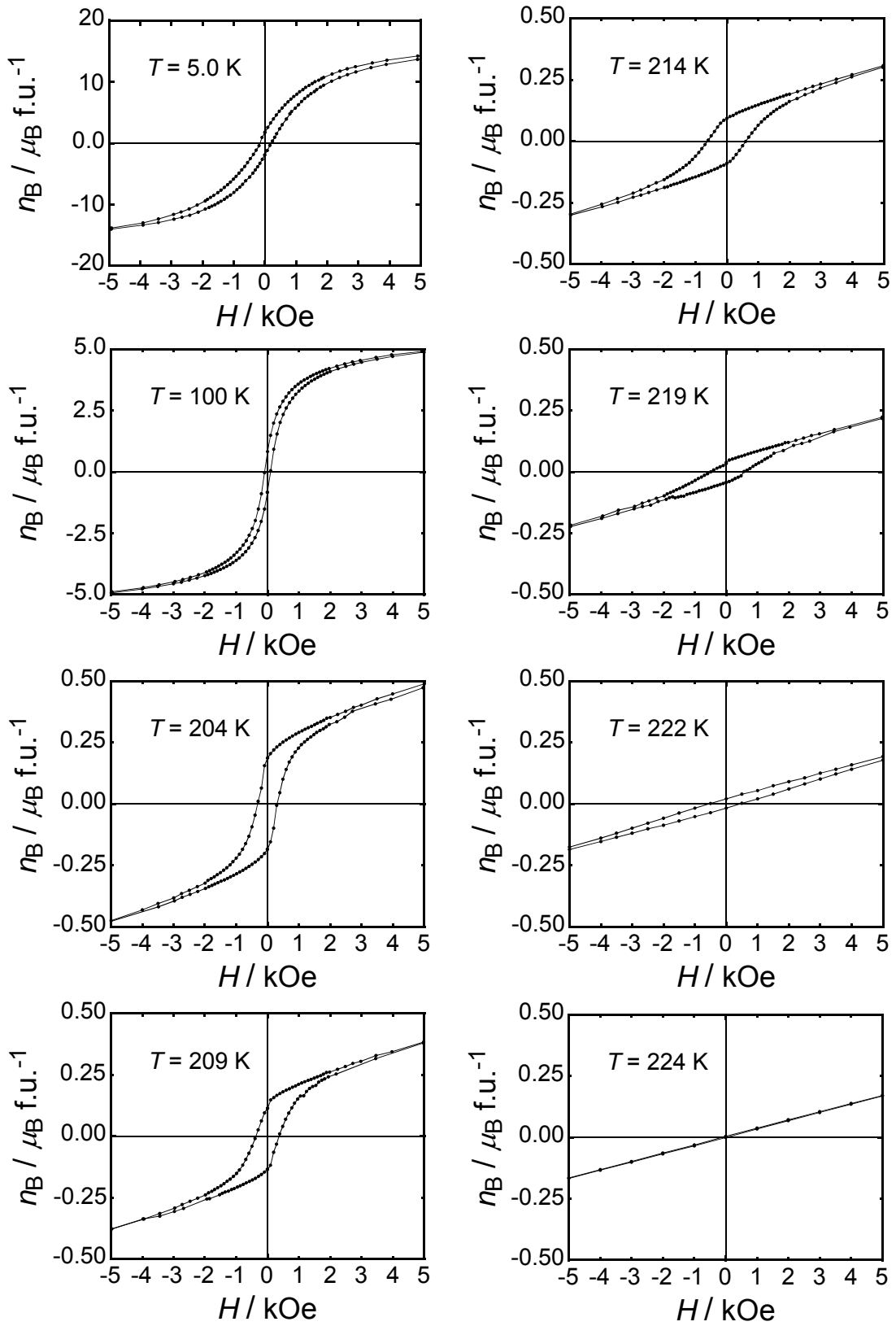## 3.4. *Hysteresis curves near T_{comp} for $Dy_3Fe_5O_{12}$*

Figure 10a and 10b display many hysteresis curves for $Dy_3Fe_5O_{12}$: (a) $T \leq T_{comp}$ and (b) $T > T_{comp}$. The magnetization curve at 224 K is a straight line, indicating T_{comp}. It should be noticed that one division of the unit for vertical axis in magnetization is different for the data at 5.0, 100 K, and 300 K from these near T_{comp} between 204 and 244 K. The gradual variation of the hysteresis curves with temperature can be seen. The maxima of H_c are given as 214 K in $T \leq T_{comp}$ and 232 K in $T > T_{comp}$.

3.5. *Temperature dependence of H_c near T_{comp} for $Dy_3Fe_5O_{12}$*

Figure 11 shows a temperature dependence of coercive force H_c for $Dy_3Fe_5O_{12}$ over the range 200 K to 250 K. The results have verified the double peak in H_c near T_{comp}. The variation itself with temperature is not smooth because of the experimental errors in the numerical values of figure 10. Nevertheless a double peak in H_c is clearly seen across T_{comp}. Table 3 denotes values of coercive force H_c for $Dy_3Fe_5O_{12}$ as a function of temperature. The maxima of H_c are given as 214 K in $T \leq T_{comp}$ and 232 K in $T > T_{comp}$. This double peak in H_c near T_{comp} is a significant characteristic which is also seen in figures 5 to 9 for R= Gd, Tb, Dy, Ho and Er.

Dy$_3$Fe$_5$O$_{12}$

(a)
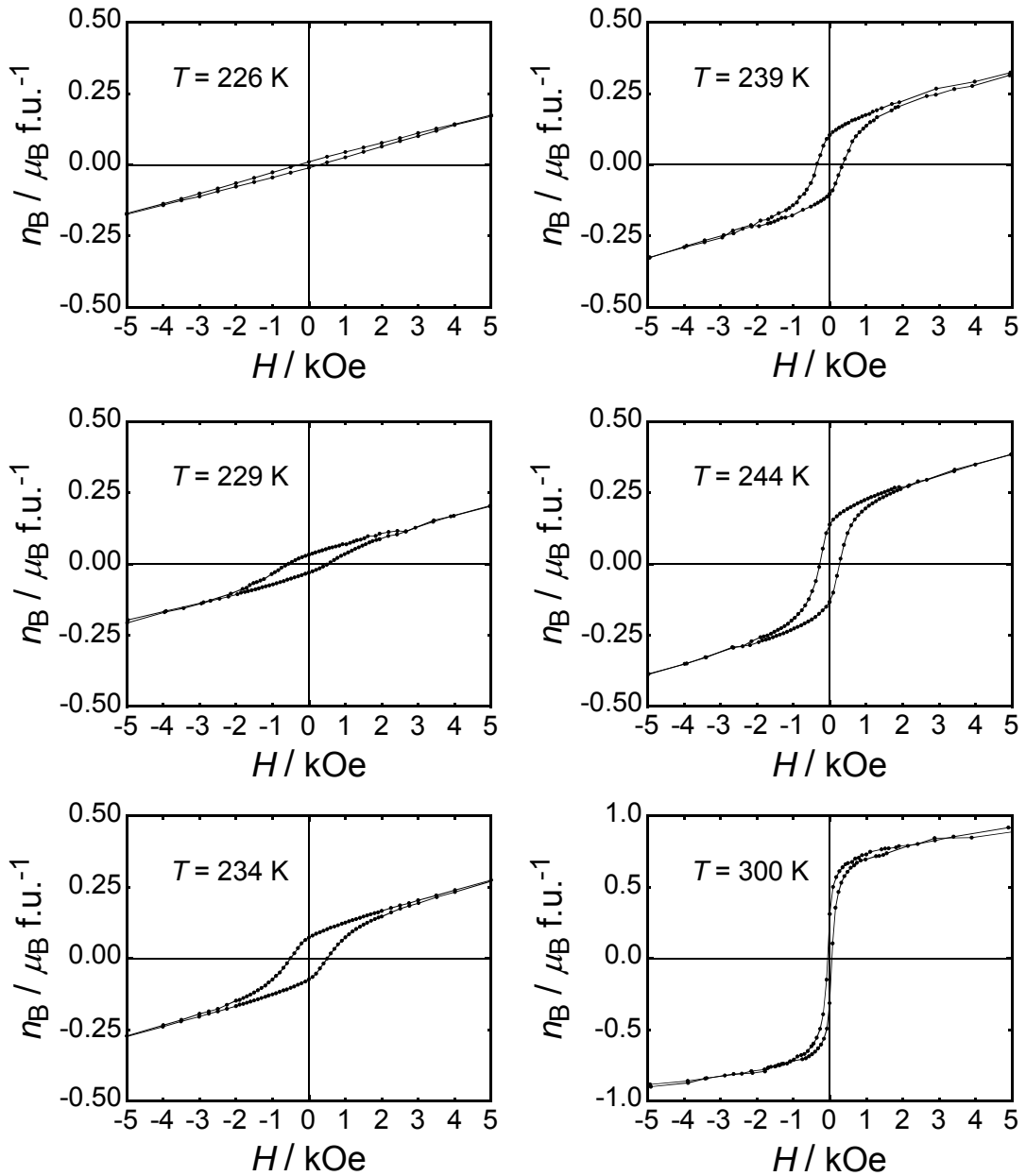
Figure 10.   Temperature dependence of the magnetic hysteresis curves (*M–H* curves) for $Dy_3Fe_5O_{12}$ (T_{comp} = 224 K). Many *M–H* curves are taken in the immediate vicinity of T_{comp} (a) T $\leq T_{comp}$ and (b) T > T_{comp}.   Note that the magnetization scales at 5.0, 100 and 300 K are different from the other curves.

Figure 12 indicates that there are two components of the magnetization for $Dy_3Fe_5O_{12}$ near T_{comp}. The observed result of (figure 12a) consists of the paraprocess contribution of Dy^{3+} ion and that from the two iron sublattices which may be almost constant near T_{comp} because of the high T_c of 559 K. The linear superimposed paraprocess contribution of Dy^{3+}

ion (figure 12b) can be estimated from the *M-H* curve at just T_{comp}. Subtraction of one from the other gives the contribution to the magnetization mainly from the iron sublattices of (figure 12c) of *A*- and *D*-sites at 214 K for $Dy_3Fe_5O_{12}$. The value of H_c is estimated to be 600 Oe and the magnetic moment n_B to be 0.13 μ_B f.u.$^{-1}$ at 5.0 kOe. The result (figure 12c) corresponds to the ferrimagnetic magnetization mainly due to iron moments in *M-H* curve.
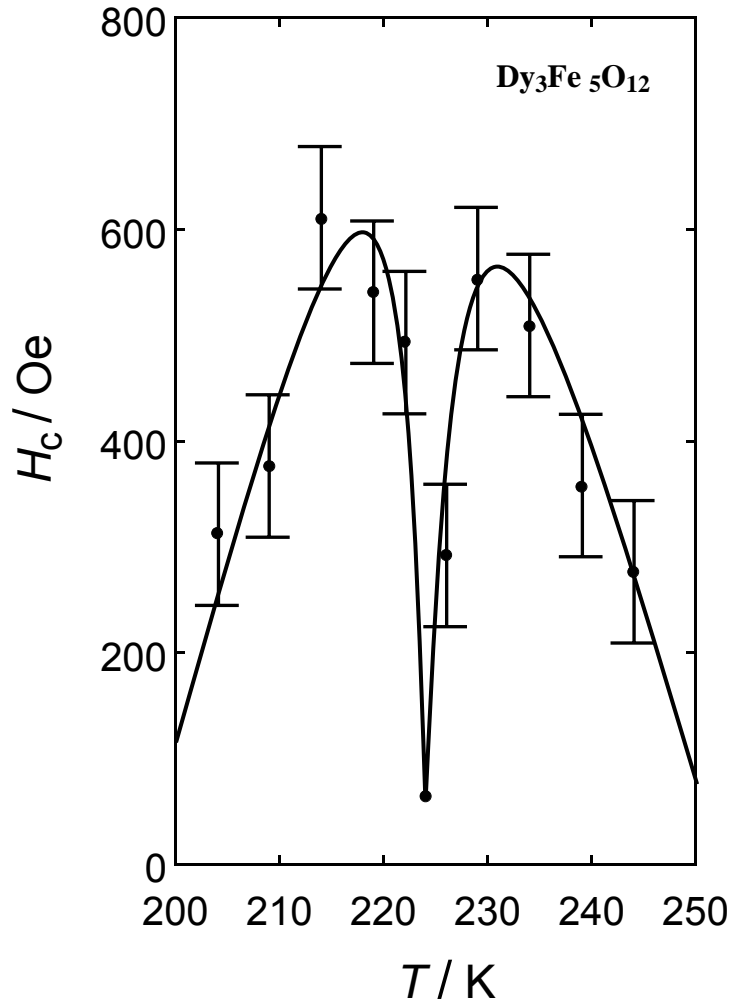
Figure 11   Temperature dependence of the coercive force H_c for $Dy_3Fe_5O_{12}$ between 200 and 250 K. A double peak of H_c has been observed at around $T_{comp}\pm$ 10 K with $T_{comp}=$ 224 K.

3.6. *Irreversible rotation of magnetization with uniaxial anisotropy*

Near T_{comp} the resultant spontaneous magnetization becomes extremely small. The demagnetizing energy could be neglected, therefore a single domain is formed and the rotation of the magnetization occurs without building up a multi-domain structure and displacement of the domain. The direct observations of the single domain structure neat

T_{comp} for $Gd_3Fe_5O_{12}$ are reported by Mee [26] and by Dillon and Earl using Faraday rotation [27]. The rapid increase of domain size has been verified as T approaches to T_{comp}. The domain size becomes extremely large and the magnetization of the sample is no longer detected near 290 K of T_{comp} [26].

Table 3. The numerical values of the coercive force H_c for $Dy_3Fe_5O_{12}$ at the different temperatures near T_{comp}.

temperature, T (K)	coercive force, H_c (Oe)
5.0	188
100	125
204	313
209	376
214	610
219	541
222	494
224	65
226	293
229	553
234	509
239	357
244	276
300	63

Let us consider a hysteresis curve arising from the single domain magnetization. The value of magnetization M_s is assumed, here, to be a constant in this simple model. A magnetic field H is applied parallel to the uniaxial easy axis. The magnitude of H is varied from $H = +2.0\ K/M_s$ to opposite direction $H = -2.0\ K/M_s$ on passing through zero. Here we define K to be a uniaxial anisotropic constant having a positive value in this model. When ϕ is defined as the angle between H and M_s, the magnetic energy E can be expressed as

$$E = K \sin^2 \phi - HM_s \cos \phi,$$ (3)

where the first term is the anisotropy energy and the second one indicates the magneto static energy.

In figure 13a, the variation of energy E is illustrated as a function of angle ϕ. The magnetization rotates suddenly from $\phi = 0$ to $\phi = \pi$ at $H = -2.0\ K/M_s$ which corresponds to H_c, and vice versa,

$$H_c = \pm\ 2.0 \frac{K}{M_s}.$$ (4)

This sequence of events leads to a rectangular-shape hysteresis loop. This value H_c increases with decreasing the magnitude of M_s. The solid circle indicates the specific angle
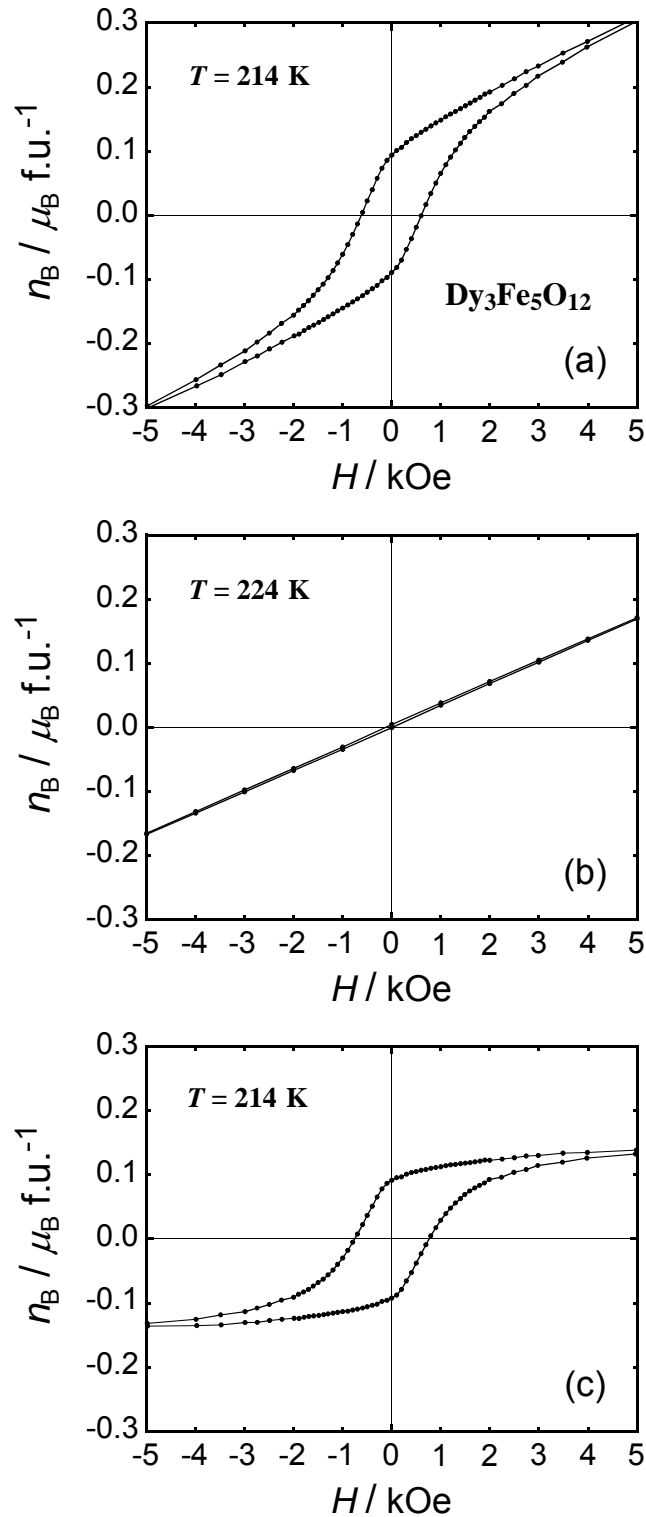
Figure 12   Two components of magnetization for $Dy_3Fe_5O_{12}$: (a) observed
             $M–H$ curve at 214 K, (b) the magnetization induced by the
             applied field at T_{comp}=224 K, and (c) the contribution which is
             mainly originated from the iron sublattices, and (c) is evaluated
             from the subtraction of (b) from (a).

ϕ at which the orientation of M_s remains at the local minimum. Let us take a value of $H =$ -1.0 K/M_s, the orientation of M_s remains at $\phi = 0$ even though the lowest energy is $\phi = \pi$. Since the energy E remains at the meta-stable state. Subsequently, figure 13b and 13c indicate that the angle between external magnetic field H and the uniaxial anisotropic easy axis is fixed to the $\pi/4$ and $\pi/2$, respectively. In figure 13b, when the field H is decreased from $H = +2.0K/M_s$ to opposite direction on passing through zero, the rotation of M_s takes place at $H = -1.0 \ K/M_s$ and $+1.0 \ K/M_s$. No jumping change in orientation is found in figure 13c.

Figure 14 shows the hysteresis curves corresponding with figure 13. The value of projection of M_s to the applied field gives the magnitude of the magnetization in figure 14. This projection is carried out at the angle specified by the location of solid circle in figure 13. The irreversible 180º rotation takes place from an easy axis to the opposite direction of M_s by increasing an applied antiparallel field in figure 13a. The simple model explains a large coercive force H_c in the M–H curve (figure 13a and 13b), respectively. The value H_c increases with decreasing the magnitude of M_s indicated in eq. (4). No hysteresis is observed for the case corresponding to figure 13c.

3.7. *A model of a double peak in H_c near T_{comp}*

Discussion for the hysteresis curve in this section will be based on the theory by Goranskiĭ and Zvezdin [24]. The main difference of this section from previous figures 13 - 14 is that the magnitude of the magnetization can vary with applied field. The variation of the magnitude of M originates from the superimposed paraprocess of the rare earth ion (R) in the iron garnets, as explained below. This paraprocess plays an important role in the hysteresis loop and an exhibition of the double peak in H_c near T_{comp}.

Let us consider a hysteresis curve on the basis of a schematic guide shown in figure 15. Suppose that the magnetic field is parallel to the easy axis of the crystal as in figure 14a. We discuss briefly a simplified model based on a single-domain structure. The total magnetization M is given by

$$M = M_{Fe} + M_R = M_{Fe} + \chi H_{eff} = M_{Fe} + \chi(H - \beta M_{Fe}) = (1 - \chi\beta) M_{Fe} + \chi H, \qquad (5)$$

where M_{Fe} denotes the resultant magnetization due to the Fe ions in its two sublattice 16A and 24D sites, as indicated in figure 1, and M_R is that of R ions. The rare earth sublattice susceptibility is introduced by the notation χ. In the neighborhood of T_{comp}, M_{Fe} does not depend on the applied field because of the extremely high T_c=559 K. On the other hand, M_R is described in terms of the Curie law with χ proportionally to $1/T$ in the first approximation. The parameter β is a constant of the exchange interaction between C-(AD) sublattices. Then we may write M down as

$$M \approx (1 - \frac{T_{\text{comp}}}{T})M_{\text{Fe}} + \frac{CH}{T} = M_0 + \chi H, \tag{6}$$

$$M_0 = (1 - \frac{T_{\text{comp}}}{T})M_{\text{Fe}}, \tag{7}$$

where C is a constant, M_0 denotes a spontaneous magnetization that vanishes at T_{comp}. Equations (6) and (7) lead to characteristic hysteresis curves near T_{comp} as follows. The minimization of magnetic energy for this model is redefined as a modified form from eq. (3) expressed as

$$E = aK \sin^2 \phi - HM \cos \phi. \tag{8}$$

The projection of the magnetization M to the external field gives the hysteresis curves as shown in figure 15, where the value of M depends on the temperature and furthermore depends on the applied field H. Here the value of a depends on the direction of the applied field with respect of the crystal axes corresponding to figure 14.

Firstly, let us take the coercive force in temperature regions of $T < T_{\text{comp}}$-δ and $T > T_{\text{comp}}$+δ, for a condition $\left|\frac{aK}{M_0}\right| < \left|\frac{M_0}{\chi}\right|$. The value of total M does not change so much by external field H in comparison with the value of M_0 within

$$|H| \leq \frac{aK}{M_0}, \tag{9}$$

therefore the coercive force H_c increases when M_0 decreases in these temperature regions. As can be seen in of figure 15a, the hysteresis curve resemble figure 14a. Here we introduce a coercive force $H_c(1)$ is given by

$$H_c(1) = \pm \frac{aK}{M_0} = \pm \frac{aK}{\left|1 - \frac{T_{\text{comp}}}{T}\right|M_{\text{Fe}}} \qquad \text{for} \quad \left|T - T_{\text{comp}}\right| > \delta. \tag{10}$$

Secondly, let us examine the temperature region of T_{comp}-δ $< T < T_{\text{comp}}$+δ, for a condition $\left|\frac{M_0}{\chi}\right| < \left|\frac{aK}{M_0}\right|$. The paraprecess contribution χH becomes larger than M_0 when

$$\frac{aK}{M_0} > |H| > \frac{M_0}{\chi} , \tag{11}$$

then the total M disappears during the reversal of the magnetization of the sample before the rotation of M_0 happens. As can be seen in figure15b, the coercive force $H_c(2)$ decreases

as T approaches to T_{comp} and is given by

$$H_c(2) = \pm \frac{M_0}{\chi} = \pm \frac{\left|1 - \frac{T_{comp}}{T}\right| M_{Fe}}{\chi} \qquad \text{for} \qquad |T - T_{comp}| < \delta. \qquad (12)$$

Consequently, the temperature δ can be determined from the equality of $H_c(1) = H_c(2)$

and the maximum of H_c can be expressed as

$$\delta \cong (\frac{T_{comp}}{M_{Fe}})(a\chi K)^{\frac{1}{2}}, \qquad (13)$$

$$H_c(\text{max}) = [H_c(1)H_c(2)]^{\frac{1}{2}} = (\frac{aK}{\chi})^{\frac{1}{2}}. \qquad (14)$$

The experimental results of $Dy_3Fe_5O_{12}$ are given as shown in figure 10. For $Dy_3Fe_5O_{12}$, the experimental measurements lead to numerical values that $T_{comp} = 224$ K, $H_c(\text{max}) = 600$ Oe at $T_{comp} \pm$ K with ≈ 10 K. The two peaks of coercive force H_c are observed at 214 and 232 K. The polycrystalline samples consist of randomly oriented grains with crystalline anisotropy. The calculation over a statistical distribution of anisotropy axis has not been made in the present analysis. The uncertainty is encountered to understand the experimental results. Two main influences of the polycrystalline samples. First, the inhomogeneity of T_{comp} of the samples may occur. Second, the orientation of the external field is not parallel to the crystalline anisotropy axis, therefore the hysteresis curves of figure 14a-14c are mixed over a statistical distribution of anisotropy axis of the specimens. The value of a becomes 4/3 along the [111] direction, 2/9 along the [100], and $4\sqrt{2}/9$ along the [110] direction [22]. Consequently, a smoothing and smearing out of the peak of H_c may be observed in the actual experiments because of compositional inhomogeneity. The anisotropy of rare earth iron garnets has been discussed and the values of anisotropy K and χ change slowly with temperature [28-31].

In the case of temperature is far from T_{comp} and the magnetization M becomes much larger, then the multi-domain structure will be built up and therefore the mixing and/or overlapping between the domain wall displacement and the rotation of the magnetization takes place. As a result the hysteresis curve will be caused by a multi-domain structure with the easy displacement of domain wall having very low value of H_c.
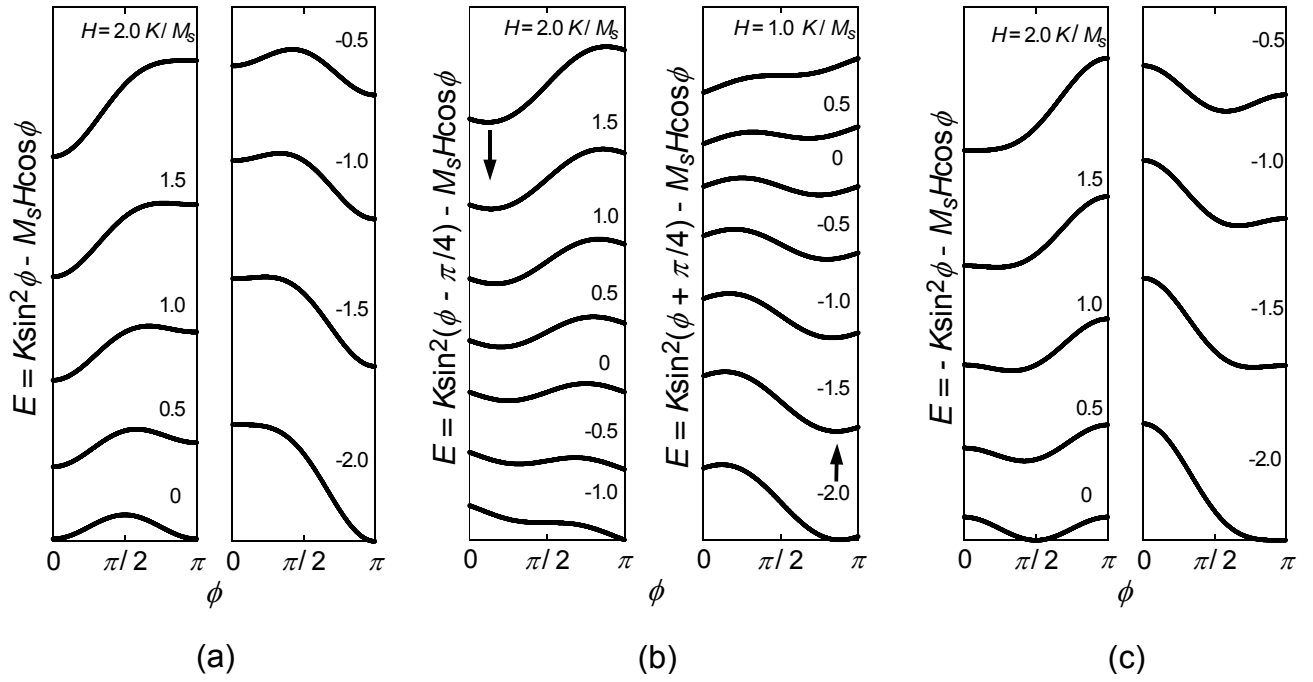
Figure 13. Variation of energy E as a function of angle ϕ between an applied magnetic field H and a magnetization M_s. The value of M_s is assumed to be constant. (a) The field is applied along the preferred direction with an anisotropy constant K. With decreasing the value of H from $H = +2.0$ K/M_s across zero to opposite direction, the magnetization rotates suddenly from $\phi = \pi$ to $\phi = 0$ at $H = -2.0$ K/M_s which corresponds to H_c. The solid circle indicates the angle ϕ at which the M_s is kept on passing hysteresis even in the metastable state. (b) The angle between the magnetic field H and the easy axis is fixed to $\pi/4$. (c) The angle is fixed to $\pi/2$.
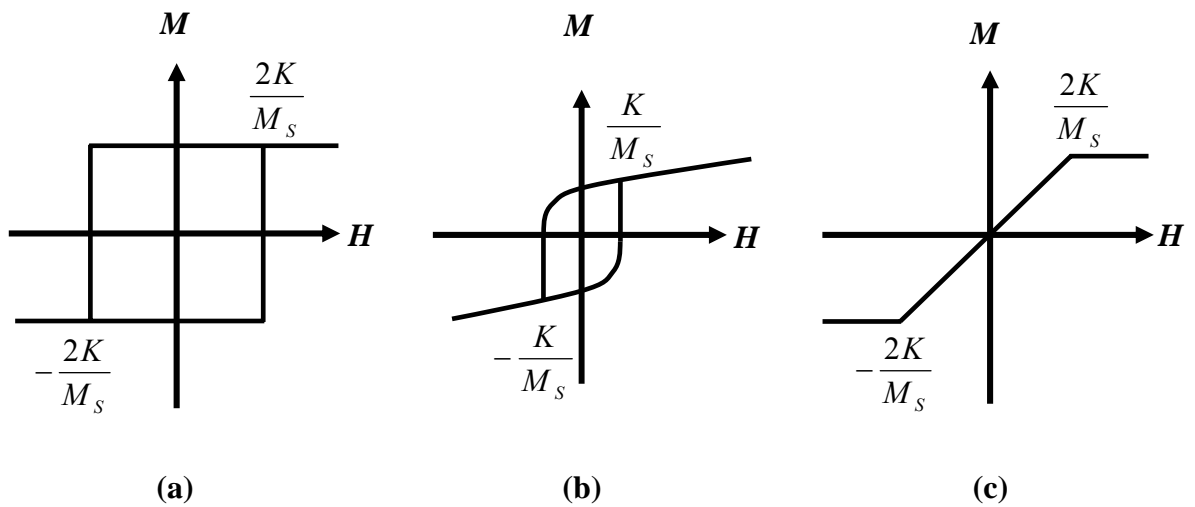
Figure 14. Hysteresis curves caused by rotation of the magnetization with the uniaxial anisotropy for single-domain model. These curves correspond to (a), (b), and (c) in figure 13. The projection of M_s to the field at ϕ specified by solid circle in figure 13 yields the magnetization M in these loops. The angle between the magnetic field H and the easy axis is fixed to (a) 0, (b) $\pi/4$ (45°), and (c) $\pi/2$ (90°), respectively.
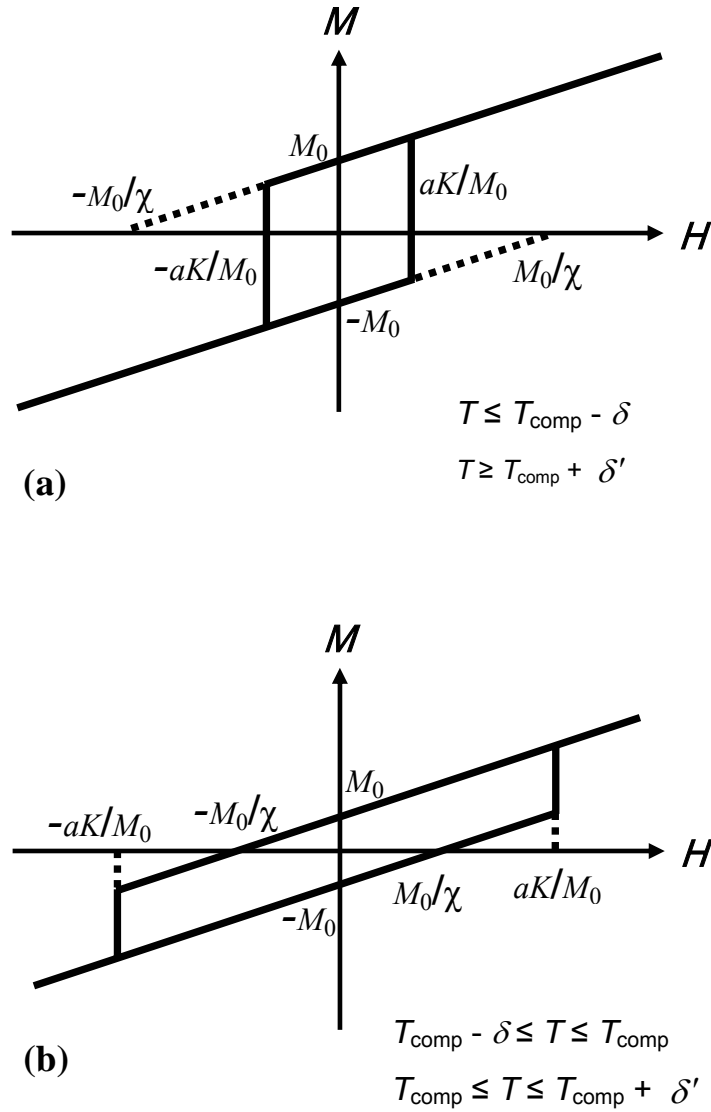
Figure 15. Hysteresis curves near T_{comp} caused by rotation of the magnetization for single-domain with uniaxial easy axis. The spontaneous magnetization is denoted by M_0 and δ is defined in text. The magnetization M is not constant but can vary with applied field. Here M is changes as $M = M_0 + \chi H$ (see text).

(a) The model is applicable for $T < T_{comp}-\delta$ and $T > T_{comp}+\delta$, for $\left|\dfrac{aK}{M_0}\right| < \left|\dfrac{M_0}{\chi}\right|$.

(b) the model is applicable for $T_{comp}-\delta \leq T \leq T_{comp}+\delta$, for $\left|\dfrac{M_0}{\chi}\right| < \left|\dfrac{aK}{M_0}\right|$

4. Summary

The present experimental results have verified systematically the double peak in coercive force H_c near T_{comp} for the polycrystalline rare earth iron garnets $R_3Fe_5O_{12}$ (R = Gd, Tb, Dy, Ho, and Er).   A model to explain is based on the hysteresis curve caused by the rotation of single domain rather than the displacements of the domain wall in the multi-domain structure. The experimental measurements lead to numerical results that   for $Dy_3Fe_5O_{12}$, T_{comp} = 224 K, H_c (max) = 600 Oe at $T_{comp} \pm$ K with   ≈ 10 K.   The basic understand of the double peak of H_c is led by the paraprocess magnetization of R^{3+} ions under influence of an external magnetic field. It should be noted that the experimental value of   is approximately 10 K and H_c (max) = 300~600 Oe for all the $R_3Fe_5O_{12}$. The appearance of the double peak of H_c (max) near T_{comp} is an inherent characteristic for $R_3Fe_5O_{12}$.

Acknowledgements

References

[1] G. Menzer, Z. Kristallogr. **69** 300 (1929).
[2] F. Bertaut and F. Forrat, Compt. Rend. **243** 382 (1956).
[3] R. Pauthenet, Compt. Rend. **243** 1499 (1956).
[4] S. Geller and M. A. Gilleo, Acta Crystallogr, **10** 239 (1957).
[5] R. Pauthenet, Annls. Phys. (Paris) **3** 424 (1958).
[6] R. Pauthenet, J. Appl. Phys. **29** 253 (1958).
[7] L. Néel, R. Pauthenet and B. Dreyfus, Prog. Low. Temp. Phys. **4** 344 (1964).
[8] E.E. Anderson, Phys. Rev. A **134** A1581 (1964).
[9] S. Geller, J.P. Remeika, R.C. Sherwood, H.J. Williams and G.P. Espinosa, Phys. Rev. **137** A1034 (1965).
[10] S. Geller, Z. Kristallogr. **125** 1 (1967).
[11] K.H. Hellwege, *Magnetic and Other Properties of Oxides and Related Compounds*. *Part A*: *Garnets and Pervskites*, edited by K.H. Hellwege, Landolt-Börnstein, Group 3 (Springer, Berlin, 1978), p.1, and references therein.
[12] S. Nagata, H. Sasaki, K. Suzuki, J. Kiuchi, and N. Wada, J. Phys. Chem. Solids, **62** 1123 (2001).
[13] J. Awaka, R. Endoh, and S. Nagata, J. Phys. Chem. Solids, **64** 2403 (2003).
[14] S. Nagata, T. Yamagishi, K. Awaka, J. Awaka, S. Ebisu, and S. Chikazawa, , *J. Phys. Chem. Solids*, **66**, 177 (2005).

[15] J. Awaka, N. Kijima, M. Uemura, Y. Kawashima, and S. Nagata, J. Phys. Chem. Solids **66** 103 (2005).

[16] J. Awaka, M. Ito, T. Suzuki, and S. Nagata, J. Phys. Chem. Solids, **66**, 851 (2005).

[17] T. Yamagishi, J. Awaka, Y. Kawashima, M. Uemura, S. Ebisu, S. Chikazawa and S. Nagata, Phil, Mag, **85** 1819 (2005).

[18] J.P. Hanton and A.H. Morrish, J. Appl. Phys. **36** 1007(1965).

[19] J.P. Hanton, IEEE Trans. Mag. **3** 505 (1967).

[20] K.P. Belov and A.V. Ped'ko, Sov. Phys. JETP **12** 666 (1961).

[21] A.V. Ped'ko, Sov. Phys. JETP **14** 505 (1962).

[22] F. Forlini and N. Minnaja, IEEE Trans. Mag. **2** 770 (1966).

[23] K.P. Belov and S.A. Nikitin, Sov. Phys. JETP **31** 505 (1970).

[24] B.P. Goranskiĭ and A.K. Zvezdin, Sov. Phys. JETP **30** 299 (1970).

[25] M. Aliev, I.K. Kamilov, M.M. Guseinov, O. Shakhshaev and A.Kh. Abduev, Russ. Phys. J. **47** 189 (2004).

[26] C.D. Mee, IBM J. of Res. and Dev. **11** 468 (1967).

[27] J.F. Dillon Jr and H.E. Earl, Am. J. Phys. **27** 201 (1959).

[28] G.P. Rodorigue, H. Meyer and R.V. Jones, J. Appl. Phys. **31** 376S (1960).

[29] R.F. Pearson, J. Appl. Phys. **33** 1236 (1962).

[30] K.P. Belov, A.K. Gapeev, R.Z. Levitin, A.S. Markosyan and Yu.F. Popov, Sov. Phys. JETP **41** 117 (1975).

[31] N.M. Kolacheva, R.Z. Levitin, B.V. Mill' and L.P. Shlyakhina Sov. Phys. solid St. **21** 604 (1979).